Acta Crystallographica Section F
Structural Biology and Crystallization Communications
ISSN 1744-3091

New insights into the binding mode of coenzymes: structure of *Thermus thermophilus* Δ^1-pyrroline-5-carboxylate dehydrogenase complexed with NADP$^+$

Eiji Inagaki,[a] Noriyasu Ohshima,[a] Keiko Sakamoto,[a] Nigar D. Babayeva,[a,b] Hiroaki Kato,[c] Shigeyuki Yokoyama[a,d,e] and Tahir H. Tahirov[a,b]*

[a]RIKEN SPring-8 Center, Harima Institute, Japan, [b]Eppley Institute for Research in Cancer and Allied Diseases, University of Nebraska Medical Center, USA, [c]Department of Structural Biology, Graduate School of Pharmaceutical Sciences, Kyoto University, Japan, [d]Department of Biophysics and Biochemistry, Graduate School of Science, University of Tokyo, Japan, and [e]RIKEN Genomic Sciences Center, Japan

Correspondence e-mail: ttahirov@unmc.edu

Received 14 March 2007
Accepted 30 April 2007

PDB Reference: Δ^1-pyrroline-5-carboxylate dehydrogenase, 2ehq, r2ehqsf.

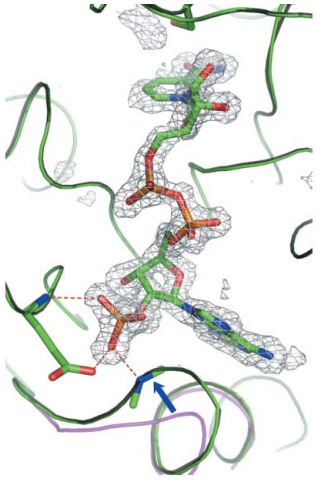

Δ^1-Pyrroline-5-carboxylate dehydrogenase (P5CDh) is known to preferentially use NAD$^+$ as a coenzyme. The k_{cat} value of *Thermus thermophilus* P5CDh (*Tt*P5CDh) is four times lower for NADP$^+$ than for NAD$^+$. The crystal structure of NADP$^+$-bound *Tt*P5CDh was solved in order to study the structure–activity relationships for the coenzymes. The binding mode of NADP$^+$ is essentially identical to that in the previously solved NAD$^+$-bound form, except for the regions around the additional 2′-phosphate group of NADP$^+$. The coenzyme-binding site can only accommodate this group by the rotation of a glutamate residue and subtle shifts in the main chain. The 2′-phosphate of NADP$^+$ increases the number of hydrogen bonds between *Tt*P5CDh and NADP$^+$ compared with that between *Tt*P5CDh and NAD$^+$. Furthermore, the phosphate of the bound NADP$^+$ would restrict the 'bending' of the coenzyme because of steric hindrance. Such bending is important for dissociation of the coenzymes. These results provide a plausible explanation of the lower turnover rate of NADP$^+$ compared with NAD$^+$.

1. Introduction

The proline metabolic pathway provides substrates for protein synthesis. However, it also often performs special functions; for example, defense against osmotic challenge in prokaryotes (Csonka, 1981) and plants (Hu *et al.*, 1992). It has been proposed that proline and its interconversions function in a mechanism for redox balance and as a mediator of redox-dependent mechanisms (Phang *et al.*, 2001). In addition, it has been suggested that the proline metabolic pathway plays an important role in p53-induced apoptosis in human cancer cells (Yoon *et al.*, 2004). Deficiencies of enzymes in the proline metabolic system cause inherited disorders such as hyperprolinemia, hypoprolinemia and hyperornithinemia with gyrate atropy (Phang *et al.*, 2001).

Δ^1-Pyrroline-5-carboxylate dehydrogenase (P5CDh; EC 1.5.1.12) is one of the key enzymes in the proline metabolic pathway. P5CDh irreversibly catalyzes the oxidation of glutamate-γ-semialdehyde (GSA) to glutamate, with the reduction of NAD$^+$ to NADH. In aqueous solution, GSA is in spontaneous equilibrium with its cyclized tautomer Δ^1-pyrroline-5-carboxylate (P5C). P5C is a precursor of proline as well as its degradation product (Phang *et al.*, 2001). P5CDh plays the primary role in the degradation of P5C; that is, the primary outflow of P5C and proline from the proline metabolic pathway. A deficiency of P5CDh causes an inherited disorder, type II hyperprolinemia (MIM 239510). Proline accumulation has been shown to induce oxidative stress *in vivo* and *in vitro*, which may be linked to the brain dysfunction observed in hyperprolinemic patients (Delwing *et al.*, 2003).

P5CDh utilizes NAD$^+$ as a coenzyme in preference to NADP$^+$. In the case of *Thermus thermophilus* P5CDh (*Tt*P5CDh), we found that the k_{cat} value for NADP$^+$ was fourfold lower than that for NAD$^+$, while the K_m values were comparable (Inagaki *et al.*, 2006). However,

Table 1
Summary of crystal data and data-collection and refinement statistics.

Values in parentheses are for the highest resolution shell.

Crystal data	
Space group	*R*3
Unit-cell parameters (Å)	a = 102.43, c = 278.84
No. of molecules in unit cell (Z)	18
Solvent content (%)	50.2
Data collection	
Source	BL44B2
Detector type	ADSC Q210
Wavelength (Å)	1.0
Temperature (K)	100
Resolution range (Å)	25–1.55 (1.59–1.55)
No. of unique reflections	158273 (10482)
Redundancy	5.7 (5.6)
Completeness (%)	100.0 (100.0)
R_{merge}	0.060 (0.435)
$\langle I/\sigma(I)\rangle$	30.9 (4.2)
Refinement statistics	
Resolution range (Å)	25–1.55
R_{work}	0.158
R_{free} (5% of reflections)	0.180
Overall average B factor excluding solvent (Å^2)	12.4
No. of atoms refined	
Protein atoms	8204
Ligand atoms	170
Solvent atoms	1060
No. of reflections used in refinement	145352
No. of reflections in test set for R_{free}	7695
R.m.s. deviations from target values	
Bond lengths (Å)	0.009
Bond angles (°)	1.2
Ramachandran plot analysis†, residues in	
Most favoured regions (%)	92.7
Additionally allowed regions (%)	7.1
Generously allowed regions (%)	0.2
Disallowed regions (%)	0.0

† Calculated using *PROCHECK* (Laskowski *et al.*, 1993).

the structural basis for the coenzyme preference was not clear. In order to understand the structural basis for the coenzyme preference, we solved the crystal structure of *Tt*P5CDh in the NADP$^+$-bound form (*Tt*P5CDh–NADP) and compared it with the crystal structure of *Tt*P5CDh in the NAD$^+$-bound form (*Tt*P5CDh–NAD) that we have reported previously (Inagaki *et al.*, 2006). The structures revealed differences in the binding mode between NADP$^+$ and NAD$^+$ and provided a structural basis for the coenzyme preference as well as further insights into the catalytic activity of the enzyme.

2. Materials and methods

2.1. Crystallization and preparation of the NADP$^+$-bound form

The methods for the expression, purification and crystallization of *Tt*P5CDh and the preparation of complex crystals have been described previously (Inagaki *et al.*, 2005). The crystals used in this study were obtained from reservoir solution containing 28–40% MPD and 50 m*M* sodium citrate buffer pH 5.2. Crystals of the NADP$^+$-bound form were prepared by a 15 min soak in solution containing 30% MPD, 5 m*M* NADP$^+$ and 50 m*M* sodium acetate buffer pH 5.2.

2.2. Data collection

A complete diffraction data set was collected at 100 K using synchrotron radiation at SPring-8 beamline BL44B2 (Hyogo, Japan). The intensity data were indexed, integrated and scaled using *DENZO* and *SCALEPACK* as implemented in the *HKL*-2000 program package (Otwinowski, 1993; Otwinowski & Minor, 1997). The crystal parameters and data-processing statistics are summarized in Table 1. Estimation of the twinning fraction (Yeates, 1997) using *DETWIN* (Taylor & Leslie, 1998) from the *CCP*4 suite (Collaborative Computational Project, Number 4, 1994) revealed the presence of hemihedral twinning (28.3%) and the data were detwinned using *DETWIN*.

2.3. Structure determination and refinement

The structure of the *Tt*P5CDh–NAD dimer (Inagaki *et al.*, 2006; PDB code 2bhp) was used as an initial model for refinement using *REFMAC*5 (Murshudov *et al.*, 1997) from the *CCP*4 suite. Model rebuilding and subsequent manual adjustments were performed using *Coot* (Emsley & Cowtan, 2004). The positions of the bound NADP$^+$ molecules were determined from the $2F_o - F_c$ and $F_o - F_c$ Fourier maps. Clear electron density was apparent for NADP$^+$ in the binding site. After refinement, additional electron density indicated an alternative conformer of the nicotinamide mononucleotide part (NMN) of NADP$^+$ extending into a solvent region. However, except for the pyrophosphate linkage part, the conformer could not be defined because of poor electron density. The disorder of NADP$^+$ was confirmed by the alternative conformations of Thr289 and Gly290, including flipping of the peptide bond between them, as found in *Tt*P5CDh–NAD; one conformer corresponds to the NMN-bound conformer, forming a hydrogen bond to the Thr289 O atom, and the other to the unbound conformer (Inagaki *et al.*, 2006).

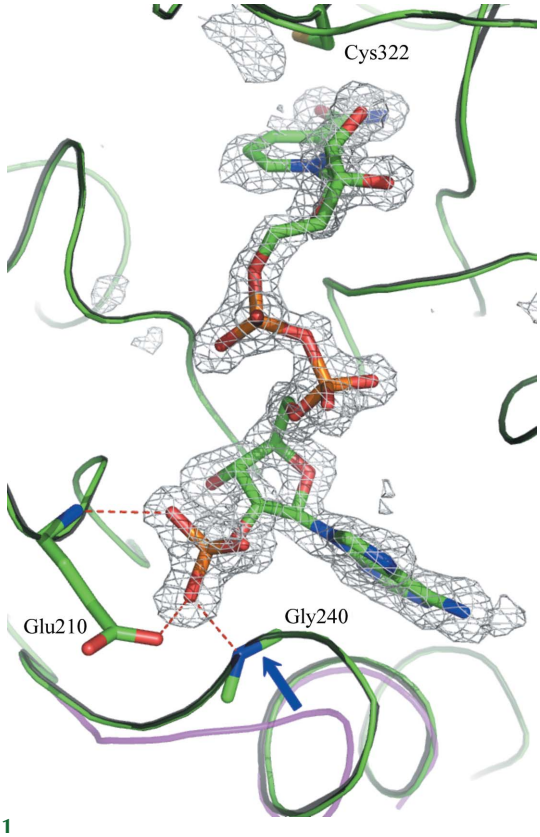

Figure 1
The binding mode of NADP$^+$. $F_o - F_c$ OMIT map of bound NADP$^+$. The catalytic cysteine (Cys322) and the Glu210 and Gly240 residues that anchor the 2′-phosphate group are shown in stick representation. The difference Fourier electron density is contoured at 3σ. The backbones of *Tt*P5CDh–NADP, *Tt*P5CDh–NAD and ligand-free *Tt*P5CDh are colored green, grey and magenta, respectively. *Tt*P5CDh–NAD and ligand-free *Tt*P5CDh were superimposed on *Tt*P5CDh–NADP.

In the proximity of Cys322 S^{γ} in *Tt*P5CDh–NADP, electron density was present that indicated a possible water molecule forming hydrogen bonds to Cys322 N and Asn184 N^{δ}. However, the presence of Cys322 as an oxidized *S*-hydroxyl form cannot be ruled out. The final refinement statistics and assessment of the model quality are summarized in Table 1. Figures were generated using *PyMOL* (DeLano, 2002).

3. Results and discussions

3.1. $NADP^+$ binding

OMIT electron-density maps clearly showed bound $NADP^+$ (Fig. 1). There are no large-scale conformational changes such as domain movements elicited by $NADP^+$ binding. The r.m.s.d. values between equivalent C^{α} atoms of *Tt*P5CDh–NADP and the ligand-free form are 0.29 Å for 514 residues (excluding two disordered N-terminal residues). A surface loop and part of the following helix (residues 238–246) undergo a large shift of up to 4.5 Å for the C^{α} atoms, which results in the closure of the adenine-binding cleft to a certain extent as shown in *Tt*P5CDh–NAD (Inagaki *et al.*, 2006; Fig. 1).

3.2. The differences in the binding modes of the coenzymes

The enzyme structure of *Tt*P5CDh–NADP is nearly identical to that of *Tt*P5CDh–NAD. The r.m.s.d. value between equivalent C^{α} atoms of *Tt*P5CDh–NADP and *Tt*P5CDh–NAD is 0.08 Å for 514 residues (excluding two disordered N-terminal residues). The bound $NADP^+$ adopts the same binding mode as NAD^+, except for the additional 2′-phosphate group of the bound $NADP^+$, which is sandwiched between Glu210 and Gly240 (Figs. 1 and 2).

With $NADP^+$, the Glu210 side chain is rotated away, with the O^{ε} and N atoms forming hydrogen bonds to the phosphate group (Fig. 1); residues 240–243 undergo subtle shifts of 0.23–0.37 Å, with Gly240 N forming a hydrogen bond. These structural modifications result in the formation of a shallow pocket which can accommodate the phosphate group in the binding site. Furthermore, the phosphate group is also stabilized by a hydrogen bond to Lys207 N^{ε} and a water-mediated hydrogen-bonding network with the residues in the binding site and other polar groups of the coenzyme (Fig. 2*a*).

3.3. Inspection of the coenzyme-binding modes for enzyme-activity study

In our previous work (Inagaki *et al.*, 2006), we proposed a catalytic mechanism for *Tt*P5CDh that would include two steps: (i) nucleophilic attack by the catalytic cysteine on the aldehyde C atom of a substrate, followed by hydride transfer to a coenzyme with production of a thioacylenzyme, and (ii) hydrolysis of the thioacylenzyme. Before step (ii), the reduced nicotinamide group of NMN would need to be displaced from the catalytic center in order to place a water molecule at the proper position of NAD^+ for hydrolysis. In addition, we also reported that the k_{cat} for $NADP^+$ is fourfold lower than that for NAD^+, while their K_m values were comparable.

In this study, it has been identified that the binding modes of $NADP^+$ and NAD^+ are essentially identical except for the regions around the ribose 2′-phosphoryl and 2′-hydroxyl groups of the adenylate parts of the coenzymes (adenosine 5′-phosphate and 2′,5′-diphosphate parts; APs), respectively. Therefore, the difference in the activity should be attributable to the differences between them. As mentioned above, the number of hydrogen bonds involving the 2′-group of $NADP^+$ is larger than that for NAD^+ (five for $NADP^+$ and three for NAD^+). In addition, the 2′-phosphate of $NADP^+$ is stabilized by three water-mediated hydrogen bonds, while the 2′-hydroxyl group is not. These interactions could retain $NADP^+$ more strongly in the binding site than NAD^+ and would therefore cause a decrease in the dissociation rate of reduced coenzyme (NADPH). As a result of this, the turnover rate of NADP(H) would be decreased.

In our previous study, the NMNs of NAD^+ in *Tt*P5CDh–NAD and NADH in the NADH-bound form (*Tt*P5CDh–NADH) revealed two types of conformers: one is the clearly identified 'binding' conformer in the NMN-binding site and the other is the poorly identified 'excluded' conformer extending into the solvent region from the pyrophosphate linkage (Figs. 3*a* and 3*b*; Inagaki *et al.*, 2006). The excluded conformers could not be defined except for the pyrophosphate linkage, indicating that they are highly disordered (Figs. 3*a* and

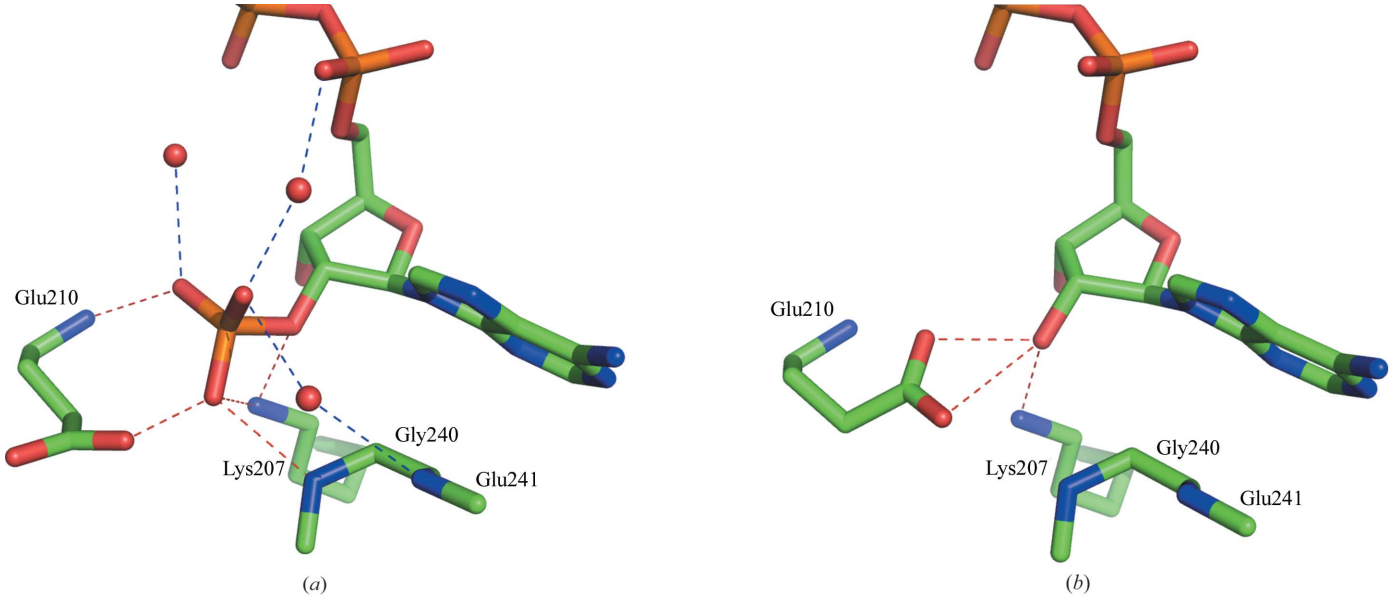

Figure 2
The differences in the binding modes between $NADP^+$ and NAD^+. Hydrogen bonds are drawn as dotted lines. The hydrogen bonds to the bound $NADP^+$ of *Tt*P5CDh–NADP (*a*) and NAD^+ of *Tt*P5CDh–NAD (*b*) are shown.

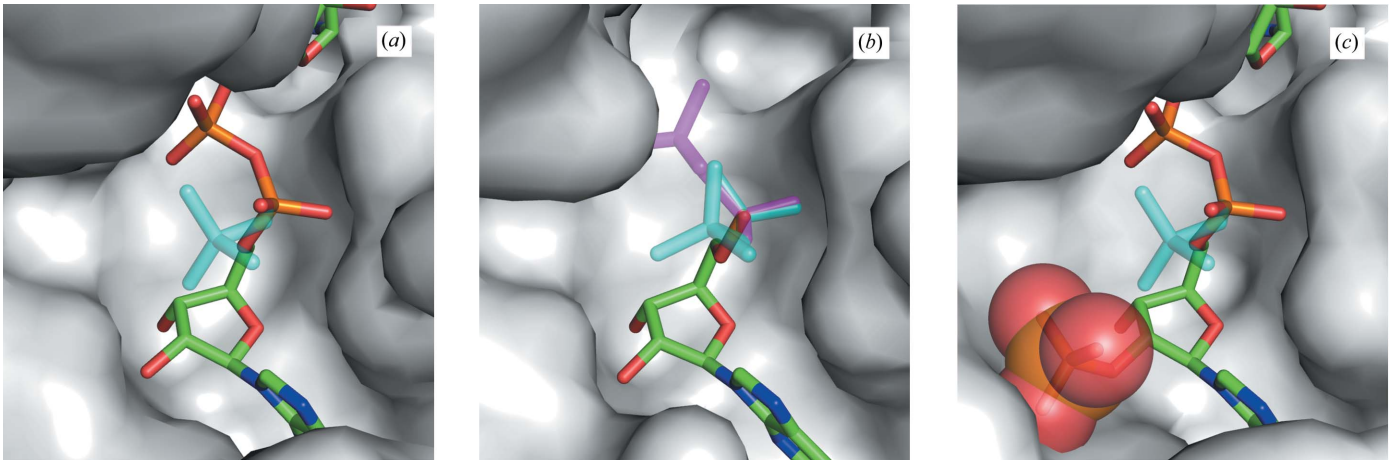

Figure 3
The coenzyme-binding pockets with 'excluded' and 'binding' conformers of bound cofactors. The NMN parts of 'excluded' conformers cannot be defined except for the bridging pyrophosphate groups. (*a*) *Tt*P5CDh–NAD with bound NAD^+: the 'excluded' conformer is colored cyan. (*b*) *Tt*P5CDh–NADH with bound NADH. It does not have a 'binding' conformer, only 'excluded' conformers (colored cyan and magenta). (*c*) *Tt*P5CDh–NADP with bound $NADP^+$: the 'excluded' conformer in *Tt*P5CDh–NAD is superimposed (colored by cyan) and the 2′-phosphate group (except for the bridging O atom) of $NADP^+$ is shown as sticks and VdW spheres.

3*b*). Meanwhile, the APs of the coenzymes can apparently be defined without disorder. These results indicate that the APs of NAD^+ and NADH can remain in the binding site despite the exclusion of the NMNs. Hence, the NMNs are expected to be displaced earlier than the APs during the enzymatic process (Inagaki *et al.*, 2006) and the exclusion of the NMNs requires a 'bend' at the pyrophosphate linkage. This indicates that this 'bending' is an important determinant of coenzyme dissociation. However, in *Tt*P5CDh–NADP, steric hindrance between the 2′-phosphate group of AP and the pyrophosphate group restrains the 'bending' of $NADP^+$. Consequently, bound $NADP^+$ cannot adopt a conformation similar to the NAD^+ conformation with the 'excluded' conformer (Fig. 3*c*).

3.4. Conclusions

A comparative analysis of the *Tt*P5CDh–NADP and *Tt*P5CDh–NAD structures suggests that (i) $NADP^+$ binds more tightly to the protein than NAD^+ and (ii) the bound NADP(H) would encounter more structural restraints than NAD(H) in the course of dissociation from the binding site. These two factors contribute to the decreased rate of NADPH dissociation compared with NADH following the enzymatic reaction, which is consistent with the results of kinetic studies for $NADP^+$ and NAD^+, *i.e.* a fourfold lower k_{cat} for $NADP^+$ than that for NAD^+.

This work was supported by the RIKEN Structural Genomics/Proteomics Initiative (RSGI), the National Project on Protein Structural and Functional Analyses, Ministry of Education, Culture, Sports, Science and Technology of Japan.

References

Collaborative Computational Project, Number 4 (1994). *Acta Cryst.* D**50**, 760–763.
Csonka, L. N. (1981). *Mol. Gen. Genet.* **182**, 82–86.
DeLano, W. L. (2002). *The PyMOL Molecular Graphics System.* http://www.pymol.org.
Delwing, D., Bavaresco, C. S., Chiarani, F., Wannmacher, C. M., Wajner, M., Dutra-Filho, C. S. & de Souza Wyse, A. T. (2003). *Brain Res.* **991**, 180–186.
Emsley, P. & Cowtan, K. (2004). *Acta Cryst.* D**60**, 2126–2132.
Hu, C. A, Delauney, A. J. & Verma, D. P. (1992). *Proc. Natl Acad. Sci. USA*, **89**, 9354–9358.
Inagaki, E., Ohshima, N., Takahashi, H., Kuroishi, C., Yokoyama, S. & Tahirov, T. H. (2006). *J. Mol. Biol.* **362**, 490–501.
Inagaki, E., Takahashi, H., Kuroishi, C. & Tahirov, T. H. (2005). *Acta Cryst.* F**61**, 609–611.
Laskowski, R. A., MacArthur, M. W., Moss, D. S. & Thornton, J. M. (1993). *J. Appl. Cryst.* **26**, 283–291.
Murshudov, G. N., Vagin, A. A. & Dodson, E. J. (1997). *Acta Cryst.* D**53**, 240–255.
Otwinowski, Z. (1993). *Proceedings of the CCP4 Study Weekend. Data Collection and Processing*, edited by L. Sawyer, N. Isaacs & S. Bailey, pp. 56–62. Warrington: Daresbury Laboratory.
Otwinowski, Z. & Minor, W. (1997). *Methods Enzymol.* **276**, 307–326.
Phang, J. M., Hu, C. A. & Valle, D. (2001). *The Metabolic and Molecular Bases of Inherited Disease*, 8th ed., edited by C. R. Scriver, A. R. Beaudet, W. Sly & D. Valle, pp. 1821–1838. New York: McGraw–Hill.
Taylor, H. O. & Leslie, A. G. W. (1998). *CCP4 Newsl.* **35**, 9.
Yeates, T. O. (1997). *Methods Enzymol.* **276**, 344–358.
Yoon, K.-A., Nakamura, Y. & Arakawa, H. (2004). *J. Hum. Genet.* **49**, 134–140.